The CASS Method for the Design of Supporting Structures

Andrea Montanino(✉) and Francesco Fabbrocino

Pegaso Telematic University, Centro Direzionale ISOLA F2, 80143 Naples, Italy
{andrea.montanino,francesco.fabbrocino}@unipegaso.it

Abstract. The understanding of the behavior of masonry structures is of fundamental importance in contemporary research, since a large portion of Europe's cultural and architectural heritage consists of masonry buildings of inestimable value, which require preservation and restoration. To this end, it is necessary to adopt technological tools capable of predicting their structural behavior, suitable for the complexity of the material. Masonry, in fact, is a peculiar material, which can be modeled as infinitely rigid in compression and incapable of resisting tension. This anisotropy makes it difficult to use standard finite element software, which instead requires a non-negligible number of parameters that are often very difficult to estimate. In this work, we present the Continuous Airy-based for Stress Singularities method (CASS) [1, 2, 3] for solving the stress field in masonry structures subjected to given forces and boundary displacements. This method is based on the minimization of complementary energy and is one of the few capable of directly providing the equilibrium solution for masonry structures. Through an appropriate variation of boundary data, it is possible to estimate the range of variability of the forces that a structure can transfer to supporting elements, such as buttresses and flying buttresses, thus enabling their design. In this way, the CASS method is proposed not only as a verification tool for existing structures, but also as a suitable design tool.

Keywords: Masonry structures · No-tension materials · Design methods · Conic optimisation

1 Introduction

The conservation and assessment of historic masonry structures -representing a substantial portion of the world's architectural heritage - have attracted growing interest within the scientific community. The development of accurate models capable of describing their mechanical behavior is essential not only for safeguarding human life but also for preserving their cultural and artistic value, particularly in relation to tourism and historical relevance [28]. Since most of these constructions are made of masonry, it is crucial to employ approaches that properly account for the distinctive mechanical features of this material.

© The Author(s), under exclusive license to Springer Nature Switzerland AG 2027
O. Gervasi et al. (Eds.): ICCSA 2026 Workshops, LNCS 16758, pp. 429–445, 2027.
https://doi.org/10.1007/978-3-032-30497-1_26

Masonry is characterized by its ability to sustain compressive stresses while being essentially unable to resist tension [19,22,23]. Standard finite element (FE) methods often prove insufficient for capturing this behavior [5,47], thus motivating the development of more advanced modeling strategies [1,40,42,44–46,48].

A fundamental contribution in this field is due to Heyman, who reformulated masonry mechanics within the framework of modern plasticity theory. This led to the introduction of simplified models such as the Normal Rigid No-Tension (NRNT) model, where masonry is treated as a continuum that can carry compression but not tension. Unlike previously mentioned approaches, which require accurate constitutive descriptions and parameter identification [10], Heyman's model does not rely on the calibration of material parameters [3,20].

One of the main challenges in the analysis of masonry structures concerns the treatment of stress singularities, i.e., regions where stresses concentrate along lines or surfaces. Within the Heyman framework, several approaches have been proposed to address this issue, both for curved structures such as domes and vaults [9,13,37], and for planar masonry systems. These include displacement-based formulations [21,25–27,29,32] as well as force-based approaches [2,4,8,31,39].

Focusing on masonry façades, the Continuous Airy-based method for Stress Singularities (CASS) has been recently introduced as an effective tool for the mesh-independent identification of stress patterns [33]. A distinctive aspect of the CASS approach is the evaluation of curvature within finite elements, which is not commonly addressed in standard formulations. Several strategies have been explored in the literature, including the use of averaged values over neighboring elements [14], as well as the adoption of higher-order plate elements, such as those employed in Isogeometric Analysis (IGA) [12], to enhance continuity and computational efficiency. However, this latter approach may introduce an artificial level of continuity in the Airy stress potential, potentially restricting the admissible solution space of the boundary value problem.

An additional advantage of the CASS method is its capability to efficiently estimate the load-bearing capacity of masonry structures by identifying the maximum load multiplier for which an equilibrated solution exists [15,30,34,38]. This also enables the determination of in-plane collapse mechanisms [6,7,11,16–18,41,43].

The stress states that can arise within masonry structures are highly varied and strongly influenced by boundary conditions, such as applied loads and support settlements, which are often difficult to determine with accuracy. Moreover, due to the hyperstatic and inelastic nature of these systems, multiple stress distributions may develop even under identical boundary conditions, all of which satisfy equilibrium and compatibility requirements [24].

The objective of this work is to exploit the capabilities of the CASS method to estimate the range of admissible stress states that can occur within a masonry structure. In particular, attention is devoted to understanding how loads are transferred to adjacent structural elements. From this perspective, the CASS

method can be interpreted as a design-oriented tool for masonry structures, enabling the proper dimensioning of supporting systems.

In the following section, the main features of the CASS method are recalled, with emphasis on its most relevant aspects, including its numerical formulation. Section 3 focuses on a practical application, where a portal structure supported by an adjacent system is introduced. By varying the boundary conditions, the study aims to evaluate the range of forces that may be transmitted to the supporting structure, thus providing useful indications for its design.

2 Boundary Value Problem

This section briefly recalls the Boundary Value Problem (BVP) for masonry structures, together with the key ingredients required for the formulation of the CASS approach.

Let $\Omega \in \mathrm{R}^2$ be the domain under consideration, as shown in Fig. 1, with boundary $\partial\Omega$ divided into a Neumann part $\partial\Omega_N$ and a Dirichlet part $\partial\Omega_D$, such that $\partial\Omega_N \cap \partial\Omega_D = \emptyset$ and $\partial\Omega_N \cup \partial\Omega_D = \partial\Omega$.

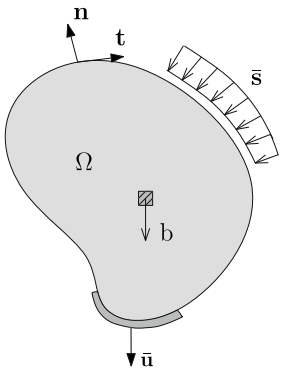

Fig. 1. Domain of the Boundary Value Problem with main notation.

The BVP over Ω is defined by equilibrium equations, kinematic relations, and a constitutive model. The equilibrium conditions are written as

$$\nabla \cdot \mathbf{T} + \mathbf{b} = \mathbf{0} \quad , \qquad \mathbf{x} \in \Omega \tag{1a}$$

$$\mathbf{T}\mathbf{n} = \bar{\mathbf{s}} \qquad \mathbf{x} \in \partial\Omega_N \tag{1b}$$

where $\mathbf{T}$ denotes the stress tensor, $\mathbf{b}$ represents body forces, $\mathbf{n}$ is the outward unit normal to the boundary, and $\bar{\mathbf{s}}$ is the prescribed traction on $\partial\Omega_N$.

The kinematic relations take the form

$$\mathbf{E} = \frac{1}{2}\left(\nabla\mathbf{u} + \nabla\mathbf{u}^T\right) \quad , \qquad \mathbf{x} \in \Omega \tag{2a}$$

$$\mathbf{u} = \bar{\mathbf{u}} \qquad \mathbf{x} \in \partial\Omega_D \tag{2b}$$

where $\mathbf{E}$ is the strain tensor, $\mathbf{u}$ the displacement field, and $\bar{\mathbf{u}}$ the imposed displacement on $\partial\Omega_D$.

The constitutive behavior of masonry is described according to Heyman's Normal, Rigid, No-Tension (NRNT) model, expressed as

$$\mathbf{T} \in \mathrm{Sym}^{-} \quad , \tag{3a}$$

$$\mathbf{E} \in \mathrm{Sym}^{+} \quad , \tag{3b}$$

$$\mathbf{T} \cdot \mathbf{E} = 0 \quad , \tag{3c}$$

where (3a) enforces the no-tension condition, (3b) expresses rigidity under compression, and (3c) represents the normality condition, corresponding to infinite friction.

The boundary value problem can be recast into a variational formulation by introducing the Total Potential Energy

$$\mathcal{E}_p(\mathbf{u}) = \frac{1}{2}\int_{\Omega} \mathbf{T} \cdot \mathbf{E} d\Omega - \int_{\partial\Omega_N} \bar{\mathbf{s}} \cdot \mathbf{u} dA - \int_{\Omega} \mathbf{b} \cdot \mathbf{u} d\Omega \tag{4}$$

or the Total Complementary Energy

$$\mathcal{E}_c(\mathbf{T}) = \frac{1}{2}\int_{\Omega} \mathbf{T} \cdot \mathbf{E} d\Omega - \int_{\partial\Omega_D} \mathbf{T}\mathbf{n} \cdot \bar{\mathbf{u}} d\Omega \tag{5}$$

These functionals allow for two alternative solution strategies [36]: minimization of the Total Potential Energy with respect to $\mathbf{u}$ leads to a displacement-based formulation, whereas minimization of the Total Complementary Energy with respect to $\mathbf{T}$ yields a force- or stress-based formulation.

In this work, the latter approach is adopted, and the problem is written as

$$\mathcal{E}_c(\mathbf{T}^*) = \min \mathbf{T} \in \mathcal{H} \mathcal{E}_c(\mathbf{T}) \quad , \tag{6}$$

with

$$\mathcal{H} = \left\{ \mathbf{T} \in \mathrm{SBV} \text{ s.t. } \mathbf{T} \in \mathrm{Sym}^{-} \, , \, \nabla \cdot \mathbf{T} + \mathbf{b} = \mathbf{0} \, , \, \mathbf{T}\mathbf{n} = \bar{\mathbf{s}} \right\} \tag{7}$$

denoting the set of admissible stress fields, i.e., fields satisfying both equilibrium conditions (1) and the material constraint (3a).

Furthermore, owing to the normality condition (3c), the functional reduces to the linear form

$$\mathcal{E}_c(\mathbf{T}) = -\int_{\partial\Omega_D} \mathbf{T}\mathbf{n} \cdot \bar{\mathbf{u}} d\Omega \tag{8}$$

In its current form, Problem (6)–(7), expressed directly in terms of the stress tensor, would lead-after discretization-to a large number of equality constraints associated with equilibrium. To avoid this issue, it is convenient to introduce the Airy stress potential F, which automatically satisfies the equilibrium equations.

The Airy stress potential is introduced as

$$\mathrm{F} \in C^0 \quad \text{s.t.} \quad \mathbf{T} = \mathbf{R}^T \mathbf{H}(\mathrm{F}) \mathbf{R} + \mathbf{B}_{\mathrm{F}} \, , \tag{9}$$

with $\mathbf{H}$ denoting the Hessian operator, $\mathbf{R}$ a skew-symmetric tensor representing a counterclockwise rotation of $\pi/2$, and $\mathbf{B}\mathrm{F}$ a tensor accounting for the body force distribution $\mathbf{b}$, such that

$$\nabla \cdot \mathbf{B}_{\mathrm{F}} = -\mathbf{b}\,. \tag{10}$$

In Cartesian coordinates, relations (9) and (10) take the form

$$\mathrm{T}_{xx} = \mathrm{F}_{,yy}\,, \quad \mathrm{T}_{yy} = \mathrm{F}_{,xx}\,, \mathrm{T}_{xy} = -\mathrm{F}_{,xy} + b_y x + b_x y\,, \tag{11}$$

where T_{xx}, T_{yy}, and T_{xy} are the Cartesian components of the stress tensor $\mathbf{T}$, and b_x, b_y are the components of the body force vector $\mathbf{b}$. A subscript following a comma denotes partial differentiation. Substitution of (11) into (10) confirms that equilibrium is identically satisfied.

Consequently, Problem (6)–(7) can be reformulated in terms of the Airy stress potential as

$$\mathcal{E}_c(\mathrm{F}^*) = \min_{\mathrm{F}\in\mathcal{H}_{\mathrm{F}}} \mathcal{E}_c(\mathrm{F}) \quad , \tag{12}$$

where $\mathcal{H}_{\mathrm{F}}$ denotes the corresponding admissible set of Airy stress potentials.

The material constraints are translated into conditions on the Hessian of F, namely

$$\mathbf{R}^T\mathbf{H}(\mathrm{F})\mathbf{R} + \mathbf{B}_{\mathrm{F}} \in Sym^{-} \tag{13}$$

which, in Cartesian coordinates, read

$$\mathrm{F}_{,xx} + \mathrm{F}_{,yy} \leq 0, \quad \mathrm{F}_{,xx}\,\mathrm{F}_{,yy} - (-\mathrm{F}_{,xy} + \mathrm{b}_{\mathrm{F}})^2 \geq 0\,. \tag{14}$$

In the absence of body forces, condition (13) admits a direct geometrical interpretation: since the Hessian governs curvature, the Airy stress potential must be pointwise concave, i.e., it must have a negative semi-definite Hessian throughout the domain.

As for the boundary conditions, the Airy-based formulation rewrites equilibrium as

$$\mathbf{R}^T\mathbf{H}(\mathrm{F})\mathbf{R}\mathbf{n} + \mathbf{B}_{\mathrm{F}}\mathbf{n} = \bar{\mathbf{s}}, \tag{15}$$

and, introducing

$$\mathrm{T}nn = \mathbf{n}\cdot\mathbf{T}\mathbf{n}\,, \quad \mathrm{T}_{nt} = \mathbf{t}\cdot\mathbf{T}\mathbf{n}, \tag{16}$$

as the normal and tangential stress components at the boundary, with $\mathbf{t}$ the tangent vector and $\mathbf{n} = \mathbf{R}\mathbf{t}$ the outward normal, the boundary conditions can be expressed as

$$\mathrm{T}_{nn} = \bar{\mathbf{s}}\cdot\mathbf{n} = \mathbf{t}\cdot\mathbf{H}(\mathrm{F})\mathbf{t} + \mathbf{n}\cdot\mathbf{B}_{\mathrm{F}}\mathbf{n} = \mathrm{F}_{,tt} - 2\mathrm{b}_{\mathrm{F}}t_x t_y \tag{17a}$$

$$\mathrm{T}_{nt} = \bar{\mathbf{s}}\cdot\mathbf{t} = -\mathbf{n}\cdot\mathbf{H}(\mathrm{F})\mathbf{t} + \mathbf{t}\cdot\mathbf{B}_{\mathrm{F}}\mathbf{n} = -\mathrm{F}_{,nt} + \mathrm{b}_{\mathrm{F}}(t_x^2 - t_y^2) \tag{17b}$$

where t_x and t_y are the Cartesian components of the tangent vector $\mathbf{t}$.

3 The Continuous Airy-Based for Stress Singularities

This section recalls the essential aspects of the numerical formulation introduced in [35], starting from the discretisation of the domain and leading to the discrete version of the optimisation problem (12).

The domain is subdivided into quadrilateral plate-type finite elements, each defined by four corner nodes, as shown in Fig. 2b. At each node, three degrees of freedom are assigned: the scalar value of the unknown function ϕ and its first derivatives with respect to the Cartesian coordinates, $\phi_{,x}$ and $\phi_{,y}$. This choice guarantees C^1 continuity at the nodes, while only C^0 continuity is ensured along element boundaries, since continuity of the normal derivative cannot be enforced between adjacent elements.

To maintain generality, each physical element is mapped onto a square reference element, referred to as the parent element, defined in the parametric coordinate system $0, s, t$, with $0 < s < 1$ and $0 < t < 1$, as illustrated in Fig. 2.

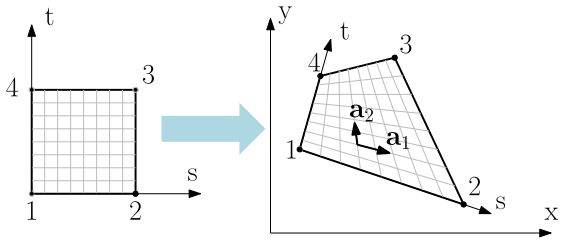

Fig. 2. Mapping between the parent and real geometries.

Since each element is associated with 12 degrees of freedom, the interpolating function $\phi(x(s,t), y(s,t))$ is constructed as the scalar product between a coefficient vector $\hat{\mathbf{w}} = [w_1, ...w_{12}]^T$ and a monomial basis

$$\mathbf{p}^T(s,t) = \left[1, s, t, s^2, st, t^2, s^3, s^2t, st^2, t^3, s^3t, st^3\right] , \tag{18}$$

such that

$$\phi(x(s,t), y(s,t)) = \mathbf{p}^T(s,t)\hat{\mathbf{w}} \quad , \tag{19}$$

The coefficient vector $\hat{\mathbf{w}}$ can be expressed in terms of the nodal degrees of freedom

$$\hat{\boldsymbol{\phi}} = [\hat{\phi}^1, \hat{\phi}^1{}_{,x}\,, \hat{\phi}^1{}_{,y}\,, ..., \hat{\phi}^4, \hat{\phi}^4{}_{,x}\,, \hat{\phi}^4{}_{,y}\,] \tag{20}$$

by enforcing interpolation conditions on the physical element. These conditions consist of 12 constraints of the form

$$\phi\Big|^i = \hat{\phi}^i\,, \quad \phi_{,x}\,\Big|^i = \hat{\phi}^i{}_{,x}\ , \quad \phi_{,y}\,\Big|^i = \hat{\phi}^i{}_{,y}\ , \tag{21}$$

with $i = 1, .., 4$, which can be written in compact form as

$$\hat{\boldsymbol{\phi}} = \mathbf{B}\hat{\mathbf{w}} \quad . \tag{22}$$

By inverting (22) and substituting into (19), the final interpolation function becomes

$$\phi(x(s,t), y(s,t)) = \mathbf{p}^T(s,t)\mathbf{B}^{-1}(\hat{\mathbf{x}})\hat{\boldsymbol{\phi}}\,. \tag{23}$$

As highlighted in Sect. 2, the computation of stresses requires the evaluation of curvature. Since curvature is not continuous at the nodes, it must be evaluated at internal locations within each element, referred to as control points. In this work, the following points in the parametric domain are selected

$$\begin{aligned} \bar{s}_1 &= 0.25\,, \quad \bar{t}_1 = 0.25 \\ \bar{s}_2 &= 0.75\,, \quad \bar{t}_2 = 0.25 \\ \bar{s}_3 &= 0.75\,, \quad \bar{t}_3 = 0.75 \\ \bar{s}_4 &= 0.25\,, \quad \bar{t}_4 = 0.75 \end{aligned} \tag{24}$$

as depicted in Fig. 3.

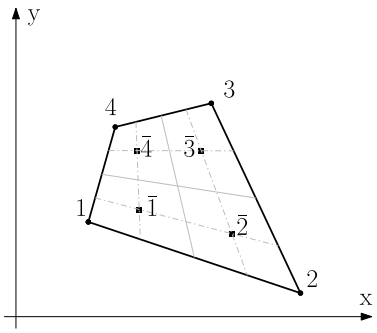

Fig. 3. Position of the control points on a generic element. The control points are placed at the centres of each quadrant in which the element is partitioned.

The Hessian tensor $\mathbf{H}(\phi)$, expressed in the curvilinear coordinate system of Fig. 2b, is written as

$$\mathbf{H} = (\nabla\phi), \alpha \otimes \mathbf{a}^\alpha\,, \tag{25}$$

where $\mathbf{a}^\alpha$, $\alpha = 1, 2$ denote the contravariant basis vectors. The projection onto the Cartesian coordinate system is then given by

$$\mathrm{H}_{ij} = [(\nabla\phi)_{,\alpha} \cdot \mathbf{e}_i](\mathbf{a}^\alpha \cdot \mathbf{e}_j)\,. \tag{26}$$

In Eqs. 25–(26), differentiation with respect to α corresponds to partial derivatives with respect to the parametric coordinates s and t.

After algebraic manipulation (see [35] for details), the Cartesian components of the curvature can be expressed in terms of the nodal degrees of freedom as

$$\begin{aligned} \phi_{,xx} &= \mathbf{h}_{xx}^T \mathbf{B}^{-1} \hat{\boldsymbol{\phi}} \\ \phi_{,yy} &= \mathbf{h}_{yy}^T \mathbf{B}^{-1} \hat{\boldsymbol{\phi}} \\ \phi_{,xy} &= \mathbf{h}_{xy}^T \mathbf{B}^{-1} \hat{\boldsymbol{\phi}} \end{aligned} \tag{27}$$

where $\mathbf{h}_{xx}$, $\mathbf{h}_{yy}$, and $\mathbf{h}_{xy}$ are vector functions depending on the parametric coordinates and the element mapping.

3.1 BVP Discretisation

Based on the formulation introduced above, the discretisation of the BVP is now addressed.

3.2 Objective Function

The Total Complementary Energy (8), expressed in terms of the Airy stress potential, is given by

$$\mathcal{E}_c(\mathrm{F}) = -\int_{\partial\Omega_D} \left(\mathbf{R}^T\mathbf{H}(\mathrm{F})\mathbf{R} + \mathbf{B}_\mathrm{F}\right)\mathbf{n}\cdot\bar{\mathbf{u}}ds, \tag{28}$$

which involves second derivatives of the unknown function, not directly included among the degrees of freedom. However, by integrating Eq. (28) along the Dirichlet boundary, one obtains, after discretisation,

$$\begin{aligned}\mathcal{E}_c(\hat{\mathbf{F}}) \quad =&[F_{,t}\,\big|_1 - F_{,t}\,\big|_2 - 2\mathrm{bF}t_x t_y \Delta s]\bar{u}_n + \\ &[F_{,n}\,\big|_2 - F_{,n}\,\big|_1 - \mathrm{b_F}(t_x^2 - t_y^2)\Delta s]\bar{u}_t\,,\end{aligned} \tag{29}$$

where $\bar{u}_t$ and $\bar{u}_n$ denote the tangential and normal boundary displacements. Summation over all the boundary elements yields the discrete objective function. The quantities $F_{,t}$ and $F_{,n}$ can be further expressed in terms of the Cartesian components of the gradient at the nodes.

3.3 Material Admissibility Constraints

The requirement of negative semi-definiteness of the stress tensor is enforced by evaluating the stress at the control points, that is, by applying (14) through (27). This leads to a set of conic constraints of the form

$$\begin{aligned}(\mathbf{h}_{xx}^T + \mathbf{h}_{yy}^T)\mathbf{B}^{-1}\hat{\mathbf{F}} \quad &\leq 0 \\ (\mathbf{h}_{xx}^T\mathbf{B}^{-1}\hat{\mathbf{F}})(\mathbf{h}_{yy}^T\mathbf{B}^{-1}\hat{\mathbf{F}}) - ((\mathbf{h}_{xy}^T\mathbf{B}^{-1}\hat{\mathbf{F}}) - b(\mathbf{x}))^2 \quad &\geq 0\end{aligned} \tag{30}$$

Collecting these relations over all control points produces a global set of conic inequality constraints, which can be written as

$$f(\hat{\mathbf{F}}) \geq \mathbf{0} \tag{31}$$

3.4 Boundary Equilibrium

The final step concerns the enforcement of the boundary conditions (17). Since second derivatives are involved, and these are not nodal variables, it is convenient to integrate the stresses along the element boundaries. In this way, equilibrium is imposed in terms of stress resultants rather than point-wise values, corresponding to an averaged equilibrium at the element level. This approximation converges to the exact condition as the mesh is refined.

Accordingly, Eq. (17) are rewritten as

$$\mathbf{R}_n = \int_{\partial\Omega_{el}} [\mathrm{F}_{,tt} - 2\mathrm{b_F} t_x t_y]\, ds \tag{32a}$$

$$\mathbf{R}_t = -\int_{\partial\Omega_{el}} \left[\mathrm{F}_{,nt} + \mathrm{b_F}(t_x^2 - t_y^2)\right] ds \tag{32b}$$

where $\mathbf{R}_n$ and $\mathbf{R}_t$ represent the normal and tangential resultants of the applied loads along the element boundary.

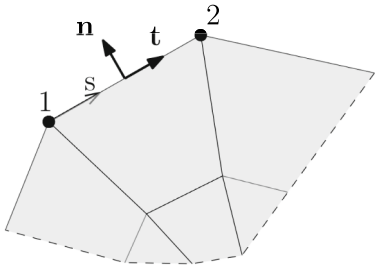

Fig. 4. Geometry of a boundary element and main notation.

After further algebraic manipulation, and expressing the relations in terms of nodal degrees of freedom, the boundary conditions at the element level are written as

$$\begin{aligned} F_{,t}\big|_2 - F_{,t}\big|_1 = {} & T_{nn}\Delta s \\ & - b_y t_x t_y (x_1 + x_2)\Delta s \\ & - b_x t_x t_y (y_1 + y_2)\Delta s \end{aligned} \tag{33}$$

$$\begin{aligned} F_{,n}\big|_2 - F_{,n}\big|_1 = {} & -T_{nt}\Delta s \\ & + \frac{1}{2} b_y (t_x^2 - t_y^2)(x_1 + x_2)\Delta s \\ & + \frac{1}{2} b_x (t_x^2 - t_y^2)(y_1 + y_2)\Delta s \end{aligned} \tag{34}$$

where Δs denotes the length of the element boundary, and x_1, x_2, y_1, y_1 are the coordinates of the endpoints, as shown in Fig. 4.

These relations can be assembled into a linear system in terms of the nodal degrees of freedom as

$$\mathbf{K}_{\partial\Omega}\hat{\mathbf{F}} = \hat{\mathbf{s}} \tag{35}$$

3.5 Discrete Boundary Value Problem

Finally, by combining Eqs. (29), (31), and (35), the discrete optimisation problem is obtained as

$$\begin{aligned} \mathcal{E}_c(\hat{\mathbf{F}}^0) \quad &= \min \mathcal{E}_c(\hat{\mathbf{F}}) \\ \text{s.t.} \qquad & f(\hat{\mathbf{F}}) \leq \mathbf{0} \\ & \mathbf{K}_{\partial\Omega}\hat{\mathbf{F}} = \hat{\mathbf{s}} \end{aligned} \tag{36}$$

3.6 Exploration of Different Equilibrium Solutions

Problem (36) is strongly driven by the objective function, that, following Eq. (29), is strongly dependent on the settlements at the Dirichlet boundary and, more in general, on boundary node displacements. From Eqs. (34), (33), and (30), it can be noticed that the existence of a solution is independent of the prescribed displacements, since the admissibility domain depends only on the geometry and prescribed boundary loads. The role of the prescribed displacement is therefore to change the objective function and localize the minimiser of the BVP, driving the solution to a new stress pattern. Furthermore, in case of vanishing boundary displacements, all solutions comprised in $\mathcal{H}$ have the same energetic level and therefore, are all admissible in terms of the requirements of the minimisation problem.

In the light of this, one possible way to explore possible stress patterns inside a structure, and therefore, the consequent load distributions on Dirichlet boundary, is to fictitiously prescribe different settlements such to drive the minimisation problem to new stress solutions.

4 Numerical Results

The proposed algorithm is applied to the portal shown in Fig. 5, with dimensions $B = 5$ m, $H = 12$ m, $h = 3$ m, $R = 3$ m; the structure is supported on its left and right pillars, and on the region S, highlighted in red in the Figure. Along this line, in fact, a supporting structure has to be designed; the structure is loaded under its self-weight, being $b = 17$ kN/m^2, and under a contact load q on the top side, being $q = 100$ kN/m.

To explore the possible stress patterns of the domain, and in particular, the reacting force on the region S, it is imagined to have a soil settlement under the left pillar, of the shape (Figs. 7 and 10)

$$\delta = \hat{u}\sin\theta\mathbf{e}_1 - \hat{v}\cos\theta\mathbf{e}_2\,. \tag{37}$$

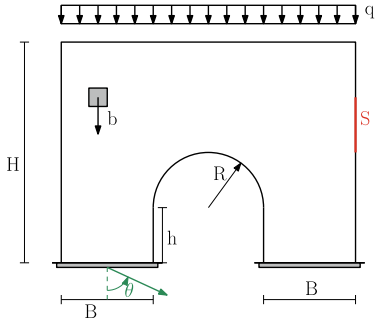

Fig. 5. Geometry and boundary conditions of the case study.

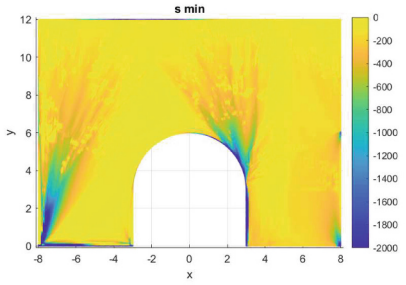

(a) Stress pattern for $\theta = 0°$

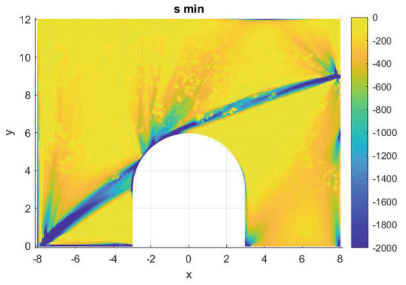

(b) Stress pattern for $\theta = 90°$

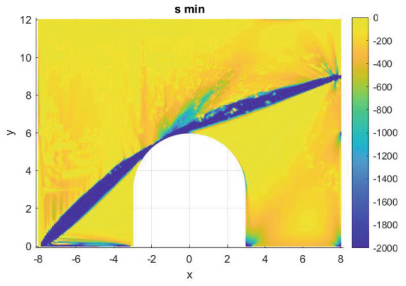

(c) Stress pattern for $\theta = 180°$

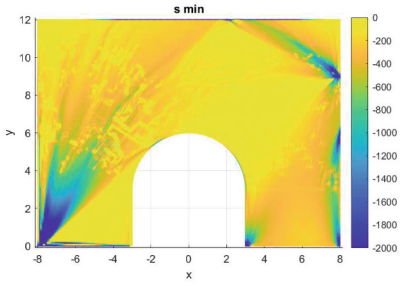

(d) Stress pattern for $\theta = 270°$

Fig. 6. Stress patterns for different boundary conditions.

Through the variation of θ in the range $[0, 2\pi]$, it is possible to explore a wide range of possible stress configurations and thus, of reacting force on the region S.

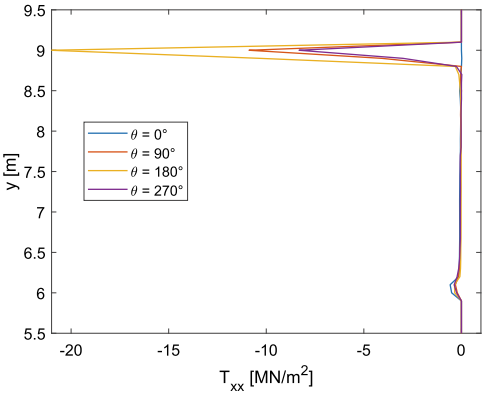

(a) Stress component σ_{xx} on the region S

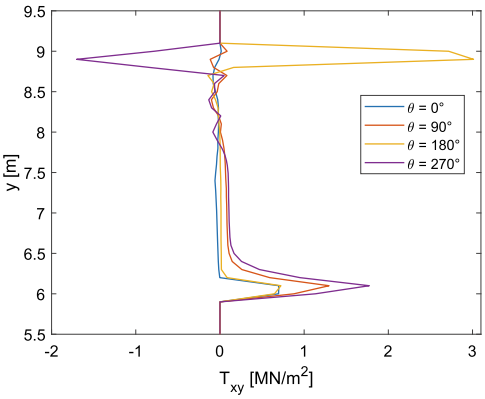

(b) Stress component σ_{xy} on the region S

Fig. 7. Emerging stress components on the region S for different value of the settlement angle θ.

In Fig. 6 the stress distribution corresponding to four representative angles are shown: in Fig. 6a, the effects of a downward settlement are depicted; in Fig. 6b, a displacement to the right is imposed; in Fig. 6c an upward settlement is imposed, while in Fig. 6d a displacement to the left is prescribed.

The corresponding emerging stress distributions in the region S are shown in Fig. 8, and more in detail, Fig. 8a represents the stress T_{xx} profile on S, while 8b represents the emerging shear stress.

Finally, Fig. 9 represents the total computed reactions on S for the whole range 0°–360°.

From these figures, it is evident the range that the supporting structure, which has its imprint on S, must sustain. In particular, the supporting structure must support a horizontal load ranging between 0 and 4000 kN, while the vertical

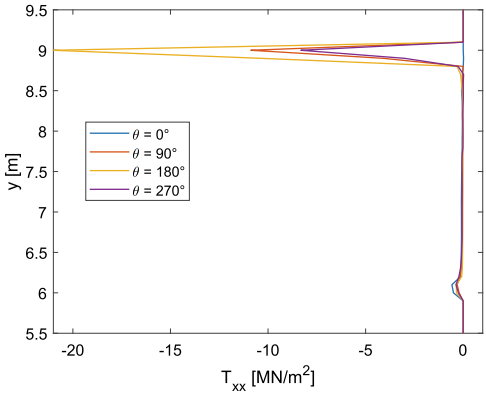

(a) Stress component σ_{xx} on the region S

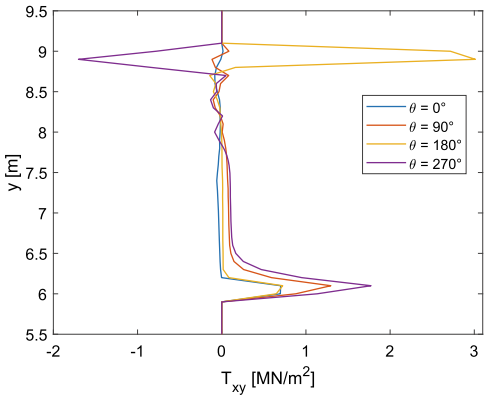

(b) Stress component σ_{xy} on the region S

Fig. 8. Emerging stress components on the region S for different value of the settlement angle θ.

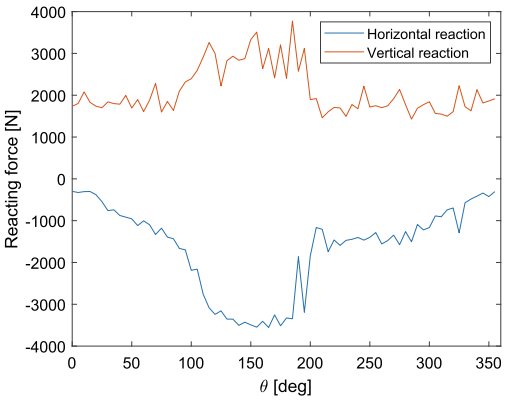

Fig. 9. Variation of the horizontal and vertical reaction force for different values of the settlement angle θ.

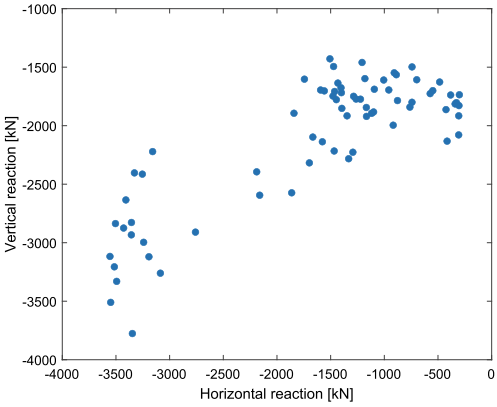

Fig. 10. Range of horizontal and vertical reaction on the region S.

reaction ranges between 1000 kN and 3500 kN. Such values must be accounted for dimensioning the related supporting structure.

5 Conclusion

In the present work, the Continuous Airy-based method for Stress Singularities has been used as a design tool for the quantification of loads on supporting structures. After introducing the boundary value problem for no-tension materials, and recalling the principal characteristics of the CASS method, with particular attention on the minimisation problem and imposition of boundary conditions, the methodology at the base of the present insight have been disclosed. In particular, the objective is to explore a wide range of stress solution, to compute the possible reaction force on contrained parts of the boundary, which may serve as imprint of supporting structure. This is done by changing fictitiously the boundary settlements in some parts of the domain, in order to generate different stress patterns.

The methodology have been finally applied to the case study of a portal, giving some imposed displacement to one of its two piers; the corresponding stress solution have been adopted to evaluate the reacting forces on a region of the right side of the portal, in order to determine which is the load that is discharged on an eventual supporting structure, as, for example, a flying buttress.

The obtained results confirm the viability of the CASS method as a monitoring tool and as a design tool. Future development will concern the exploration of alternative ways to increase the range of investigated stress pattern, to have a more precise perspective on the behaviour of the structure under investigation.

References

1. Alfano, G., Rosati, L., Valoroso, N.: A numerical strategy for finite element analysis of no-tension materials. Int. J. Numer. Meth. Eng. **48**(3), 317–350 (2000). https://doi.org/10.1002/(SICI)1097-0207(20000530)48:33.0.CO;2-C
2. Angelillo, M.: Constitutive relations for no-tension materials. Meccanica **28**, 195–202 (1993). https://doi.org/10.1007/BF00989121
3. Angelillo, M. (ed.): Mechanics of Masonry Structures. CICMS, vol. 551. Springer, Vienna (2014). https://doi.org/10.1007/978-3-7091-1774-3
4. Baratta, A., Corbi, O.: Stress analysis of masonry vaults and static efficacy of FRP repairs. Int. J. Solids Struct. **44**(24), 8028–8056 (2007). https://doi.org/10.1016/j.tafmec.2005.09.008
5. Block, P., Ciblac, T., Ochsendorf, J.: Real-time limit analysis of vaulted masonry buildings. Comput. Struct. **84**(29–30), 1841–1852 (2006). https://doi.org/10.1016/j.compstruc.2006.08.002
6. Buzzetti, M., Gandolfi, A., Pingaro, N., Milani, G.: A new advanced and simple procedure for the nonlinear static analysis of curved masonry structures. In: Mazzolani, F.M., Landolfo, R., Faggiano, B. (eds.) IPROHITECH 2025. LNCE, vol. 596, pp. 176–183. Springer, Cham (2025). https://doi.org/10.1007/978-3-031-87316-4_22
7. Buzzetti, M., Pingaro, N., Gandolfi, A., Milani, G.: Limit analysis-based approach for the assessment of local failures in masonry aggregates according to Italian standards. In: Mazzolani, F.M., Landolfo, R., Faggiano, B. (eds.) PROHITECH 2025. LNCE, vol. 596, pp. 168–175. Springer, Cham (2025). https://doi.org/10.1007/978-3-031-87316-4_21
8. Cuomo, M., Ventura, G.: A complementary energy formulation of no tension masonry-like solids. Comput. Methods Appl. Mech. Eng. **189**(1), 313–339 (2000). https://doi.org/10.1016/S0045-7825(99)00298-4
9. Cusano, C., Montanino, A., Olivieri, C., Paris, V., Cennamo, C.: Graphical and analytical quantitative comparison in the Domes assessment: the case of San Francesco di Paola. Appl. Sci. **11**(8), 3622 (2021)
10. Di Gennaro, L., et al.: In-situ load testing of an ancient masonry structure using fibre optics. Structures **70**, 107567 (2024)
11. Fabbrocino, F., Olivieri, C., Luciano, R., Vaiano, G., Maddaloni, G., Iannuzzo, A.: Seismic performance of historic masonry buildings: A comparative analysis of equivalent frame and block-based methods. Alex. Eng. J. **109**, 359–375 (2024)
12. Farahat, A., Verhelst, H.M., Kiendl, J., Kapl, M.: Isogeometric analysis for multi-patch structured Kirchhoff-Love shells. Comput. Methods Appl. Mech. Eng. **411**, 116060 (2023)
13. Fraddosio, A., Lepore, N., Piccioni, M.D.: Thrust surface method: an innovative approach for the three-dimensional lower bound limit analysis of masonry vaults. Eng. Struct. **202**, 109846 (2020)
14. Fraternali, F., Angelillo, M., Fortunato, A.: A lumped stress method for plane elastic problems and the discrete-continuum approximation. Int. J. Solids Struct. **39**(25), 6211–6240 (2002)
15. Galassi, S., Ruggieri, N., Tempesta, G.: A novel numerical tool for seismic vulnerability analysis of ruins in archaeological sites. Int. J. Arch. Heritage **14**(1), 1–22 (2020). https://doi.org/10.1080/15583058.2018.1492647

16. Galassi, S., Tempesta, G.: Safety assessment of masonry undamaged and damaged arches subjected to gravitational loads and horizontal forces: a numeric procedure to identify the optimal thrust line. Int. J. Solids Struct. **301**, 112943 (2024). https://doi.org/10.1016/j.ijsolstr.2024.112943
17. Galassi, S., Zampieri, P.: A new automatic procedure for nonlinear analysis of masonry arches subjected to large support movements. Eng. Struct. **276**, 115359 (2023). https://doi.org/10.1016/j.engstruct.2022.115359
18. Galassi, S.: An alternative approach for limit analysis of masonry arches on moving supports in finite small displacements. Eng. Fail. Anal. **145**, 107004 (2023)
19. Guadagnuolo, M., Di Gennaro, L., Basile, A., De Matteis, G.: Simplified methods for the evaluation of mechanical properties of tuff masonry walls in Campania (Italy). Procedia Struct. Integrity **44**, 878–885 (2023)
20. Heyman, J.: The stone skeleton. Int. J. Solids Struct. **2**(2), 249–279 (1966). https://doi.org/10.1016/0020-7683(66)90018-7
21. Hua, Y., Buzzetti, M., Pingaro, N., da Silva, L.C., Milani, G.: A computerized tool for the kinematic limit analysis of 2D masonry structures failing on a tilting table. SoftwareX **30**, 102180 (2025)
22. Huerta, S.: The analysis of masonry architecture: a historical approach: to the memory of professor Henry. J. Cowan. Arch. Sci. Rev. **51**(4), 297–328 (2008). https://doi.org/10.3763/asre.2008.5136
23. Huerta Fernández, S.: Mechanics of masonry vaults: the equilibrium approach (2001)
24. Iannuzzo, A., Gesualdo, A., Olivieri, C., Montanino, A.: 3D exploration of internal stresses due to lateral loads and foundation movements in a semicircular arch. In: Computational Methods in Structural Dynamics and Earthquake Engineering, pp. 2476–2491. National Technical University of Athens (2023)
25. Iannuzzo, A., Musone, V., Ruocco, E.: A neural network-based automated methodology to identify the crack causes in masonry structures. Comput.-Aided Civ. Infrastruct. Eng. **39**(24), 3769–3785 (2024)
26. Iannuzzo, A., Block, P., Angelillo, M., Gesualdo, A.: A continuous energy-based numerical approach to predict fracture mechanisms in masonry structures: CDF method. Comput. Struct. **257**, 106645 (2021). https://doi.org/10.1016/j.compstruc.2021.106645
27. Iannuzzo, A., Mallardo, V.: A novel approach to model differential settlements and crack patterns in masonry structures. Eng. Struct. **323**, 119220 (2025)
28. Iannuzzo, A., Matarazzo, G., Cusano, C., Ferraro, M., Maddaloni, G.: Insights into the collapse of the asciello masonry bridge in benevento. In: Gervasi, O., et al. (eds.) ICCSA 2025. LNCS, vol. 15886, pp. 381–395. Springer, Cham (2025). https://doi.org/10.1007/978-3-031-97576-9_26
29. Iannuzzo, A., Mele, T.V., Block, P.: Stability and load-bearing capacity assessment of a deformed multi-span masonry bridge using the PRD method. Int. J. Masonry Res. Innov. **6**(4), 422–445 (2021). https://doi.org/10.1504/IJMRI.2021.118842
30. Iannuzzo, A., Montanino, A.: A limit analysis-based CASS approach for the in-plane seismic capacity of masonry façades. Int. J. Solids Struct. **289**, 112633 (2024). https://doi.org/10.1016/j.ijsolstr.2023.112633
31. Lucchesi, M., Šilhavỳ, M., Zani, N.: A new class of equilibrated stress fields for no-tension bodies. J. Mech. Mater. Struct. **1**(3), 503–539 (2006). https://doi.org/10.2140/jomms.2006.1.503
32. Meloni, G., Pourfouladi, M., Pingaro, N.: Parametric modelling and nonlinear FE analysis of trepponti bridge subjected to differential settlements. Buildings **16**, 47 (2026). https://doi.org/10.3390/buildings16010047

33. Montanino, A., De Gregorio, D., Olivieri, C., Iannuzzo, A.: The continuous airy-based for stress-singularities (CASS) method: an energy-based numerical formulation for unilateral materials. Int. J. Solids Struct. **256**, 111954 (2022). https://doi.org/10.1016/j.ijsolstr.2022.111954
34. Montanino, A., Fabbrocino, F.: Seismic performance of irregular buildings through the CASS method. In: Gervasi, O., et al. (eds.) ICCSA 2025. LNCS, vol. 15886, pp. 338–353. Springer, Cham (2025). https://doi.org/10.1007/978-3-031-97576-9_23
35. Montanino, A., Iannuzzo, A.: A quadrilateral plate-type finite element to model stress singularities in no-tension materials. Comput. Methods Appl. Mech. Eng. **432**, 117433 (2024)
36. Montanino, A., Olivieri, C., De Gregorio, D., Iannuzzo, A.: Two continuous dual strategies to solve the kinematical and equilibrium problem for masonry-like structures. WCCM-ECCOMAS CONGRESS. Scipedia SL (2022)
37. Montanino, A., Olivieri, C., Zuccaro, G., Angelillo, M.: From stress to shape: equilibrium of cloister and cross vaults. Appl. Sci. **11**(9), 3846 (2021)
38. Montanino, A., Perelli, F.L., De Gregorio, D., Zuccaro, G.: Application of the continuous airy-based for stress singularities (CASS) to the load bearing capacity of masonry structures under seismic loads (2023)
39. Nodargi, N.A.: An isogeometric collocation method for the static limit analysis of masonry domes under their self-weight. Comput. Methods Appl. Mech. Eng. **416**, 116375 (2023). https://doi.org/10.1016/j.cma.2023.116375
40. Paris, V., Gobbin, F., Nannei, V.M., Resmini, M., Mirabella Roberti, G.: Distinct element method analyses for damage assessment: the northern spur of valverde bulwark in the venetian fortress of bergamo. Int. J. Arch. Heritage 1–15 (2024)
41. Perelli, F.L., De Gregorio, D., Montanino, A., Olivieri, C., Maddaloni, G., Iannuzzo, A.: Energy-based modelling of in-plane fragility curves for the 2D ultimate capacity of Italian masonry buildings. Front. Built Environ. **9**, 1127523 (2023)
42. Petracca, M., Camata, G., Spacone, E., Pelà, L.: Efficient constitutive model for continuous micro-modeling of masonry structures. Int. J. Arch. Heritage **17**(1), 134–146 (2023). https://doi.org/10.1080/15583058.2022.2124133
43. Pingaro, N., Milani, G.: Simple interface element equipped with thickness for the non-linear static heterogeneous analysis of masonry walls in-plane loaded: implementation and validation. Eng. Struct. **351**, 122056 (2026). https://doi.org/10.1016/j.engstruct.2025.122056
44. Prosperi, A., Longo, M., Korswagen, P.A., Korff, M., Rots, J.G.: Sensitivity modelling with objective damage assessment of unreinforced masonry façades undergoing different subsidence settlement patterns. Eng. Struct. **286**, 116113 (2023). https://doi.org/10.1016/j.engstruct.2023.116113
45. Rotunno, T., Fagone, M., Ranocchiai, G., Grande, E.: Micro-mechanical FE modelling and constitutive parameters calibration of masonry panels strengthened with CFRP sheets. Compos. Struct. **285**, 115248 (2022). https://doi.org/10.1016/j.compstruct.2022.115248
46. Shadlou, M., Ahmadi, E., Kashani, M.M.: Micromechanical modelling of mortar joints and brick-mortar interfaces in masonry Structures: a review of recent developments. Structures **23**, 831–844 (2020)
47. Shin, H.V., Porst, C.F., Vouga, E., Ochsendorf, J., Durand, F.: Reconciling elastic and equilibrium methods for static analysis. ACM Trans. Graphics (TOG) **35**(2), 1–16 (2016). https://doi.org/10.1145/2835173
48. Xia, Q., Sun, Y., Wu, J., Li, J., Li, Y., Shen, C.: Investigation of compression constitutive relationship of ancient brick masonry. Constr. Build. Mater. **317**, 126093 (2022). https://doi.org/10.1016/j.conbuildmat.2021.126093